Am J Physiol Heart Circ Physiol 299: H898–H907, 2010.
First published June 18, 2010; doi:10.1152/ajpheart.00353.2010.

Characterization of the relationship between systolic shear strain and early diastolic shear strain rates: insights into torsional recoil

Richard B. Thompson,[1] Ian Paterson,[2] Kelvin Chow,[1] June Cheng-Baron,[1] Jessica M. Scott,[3] Ben T. Esch,[3] Daniel B. Ennis,[4] and Mark J. Haykowsky[3]

[1]*Department of Biomedical Engineering,* [2]*Division of Cardiology, and* [3]*Department of Physical Therapy, University of Alberta, Edmonton, Alberta, Canada; and* [4]*Department of Radiological Sciences, University of California, Los Angeles, California*

Submitted 7 April 2010; accepted in final form 16 June 2010

Thompson RB, Paterson I, Chow K, Cheng-Baron J, Scott JM, Esch BT, Ennis DB, Haykowsky MJ. Characterization of the relationship between systolic shear strain and early diastolic shear strain rates: insights into torsional recoil. *Am J Physiol Heart Circ Physiol* 299: H898–H907, 2010. First published June 18, 2010; doi:10.1152/ajpheart.00353.2010.—Early diastolic left ventricular (LV) untwisting has been evaluated as a manifestation of LV recoil, reflecting the release of elastic energy stored during systole. The primary goal of this study was to characterize the relationship between systolic strain (e.g., circumferential strain and the shear strains that comprise twist) with the resulting early diastolic shear strain rates, including the rate of untwisting. A further goal was to characterize these relationships regionally from apical to basal locations. Cardiac magnetic resonance imaging tissue tagging was used to measure circumferential strain, global and regional (apex, mid, basal) twist (θ), and circumferential-longitudinal (ϵ_{CL}) and circumferential-radial (ϵ_{CR}) shear strains along with the corresponding untwisting rates ($d\theta/dt$) and diastolic shear strain rates ($d\epsilon/dt$) in 32 healthy males (33 ± 7 yr). LV untwisting rates and shear strain rates measured during early diastole varied significantly with the measurement location from apex to base ($P < 0.001$) but demonstrated significant linear correlation with their corresponding preceding systolic strains ($P < 0.001$). Untwisting rates and diastolic shear strain rates were not significantly correlated with circumferential systolic strain or end-systolic volume ($P > 0.05$). Normalization of the untwisting rates to the peak twist ($d\theta/dt_{Norm} = -13.6 \pm 2.1\ s^{-1}$) or shear strain rates to peak systolic shear strain ($d\epsilon_{CL}/dt_{Norm} = -15.0 \pm 5.4\ s^{-1}$, and $d\epsilon_{CR}/dt_{Norm} = -14.2 \pm 7.7\ s^{-1}$) yielded a uniform measure of early diastolic function that was similar for all shear strain and twist components and for all locations from apex to base. These findings support a linear model of torsional recoil in the healthy heart, where diastolic shear strain rates (e.g., untwisting rates) are linearly related to the corresponding preceding systolic shear stain component. Furthermore, these findings suggest that torsional recoil is uncoupled from end-systolic volumes or the associated strains, such as circumferential strain.

relaxation; torsion; untwisting

LEFT VENTRICULAR (LV) twist during systole and subsequent untwisting during diastole are a consequence of the characteristic helical muscle fiber orientations and their variations from endo- to epicardium (15, 29). These fiber orientations facilitate uniform transmural fiber shortening and wall stress (1), thereby improving the efficiency of ventricular systolic function. This geometry also accommodates changes in fiber length at constant ventricular volume, during isovolumic relaxation, as changes in shear strain (2). For example, ~40% of ventricular untwisting, which is associated with the circumferential-longitudinal shear strain (ϵ_{CL}) component, is completed during isovolumic relaxation in the normal heart at rest (10, 12, 22). Because shear strains such as untwisting are the predominant deformation during early diastole, they have been evaluated as a measure of ventricular relaxation by direct comparison to isovolumic pressure decay time constant (τ) (5, 10, 23, 27, 32, 34). Whereas the peak rate of untwisting was shown to correlate with τ in animal studies [Dong et al. (10), $R = -0.86$; Wang et al. (34), $R = -0.81$; and Notomi et al. (23), $R = -0.66$], human studies have shown less (34) ($R = -0.51$) or no significant correlation (5). There is much stronger evidence for LV untwisting as a manifestation of torsional recoil (2, 3, 6, 17, 22, 23, 32, 36), given the significant correlation between the early diastolic untwisting rate and peak systolic twist in humans (8, 16, 22, 25, 35) and the correlation of untwisting rates with end-systolic volumes (ESVs) (3, 35). Linear correlations between peak twist and untwisting rates have been observed in several studies (8, 16, 22, 25, 35), but this systolic-diastolic relationship has not been evaluated for the more fundamental shear strains, nor has it been evaluated regionally. We propose that the shear strains developed during systole are linearly related to the subsequent corresponding shear strain rates during early diastole and thus that a simple linear model of torsional recoil describes the link between systole and early diastolic function. Systolic shear strains are heterogeneous in humans (4, 18), and thus regional variations in the diastolic shear strains rates (and untwisting rates) would be expected. The goals of this current study were, first, to measure diastolic shear strain rates in the healthy heart and to characterize their relationship with the preceding systolic shear strains as well as with systolic circumferential strains and ventricular volumes. A second goal was to determine whether these relationships are maintained as a function of the position in the ventricle despite the expected heterogeneity of systolic shear strains.

METHODS

Study Population

The protocol for examining subjects using cardiac MRI (cMRI) was approved by the Health Research Ethics Board at the University of Alberta, and all patients signed statements of informed consent before being examined. Thirty-two healthy adult male volunteers (33 ± 7 yr) underwent a cMRI exam to measure LV volumes and function. The subject characteristics are summarized in Table 1. None of the subjects had a history of heart disease.

Address for reprint requests and other correspondence: R. B. Thompson, Dept. of Biomedical Engineering, 1082 Research Transition Facility, Univ. of Alberta, Edmonton, AB, T6G 2V2, Canada (e-mail: richard.thompson@ualberta.ca).

Table 1. *Participant characteristics*

Participants/female	32/0
Age, yr	33 ± 7
Range	19–42
Body surface area, m^2	2.0 ± 0.2
Heart rate, beats/min	62.7 ± 12.3
Systolic blood pressure, mmHg	121.0 ± 5.1
Diastolic blood pressure, mmHg	74.1 ± 6.9
LVEDV, ml	171.9 ± 31.1
LVESV, ml	71.1 ± 15.6
LV SV, ml	101.3 ± 21.0
LV EF, %	62.1 ± 3.1
LV mass, g	146.2 ± 22.1
LV length, cm	10.9 ± 0.7
LV length (end systole), cm	8.6 ± 0.5

Values are means ± SD. LVEDV, left ventricular (LV) end-diastolic volume; LVESV, LV end-systolic value; SV, stroke volume; EF, ejection fraction.

Magnetic Resonance Imaging

Data acquisition. All cMRI examinations were performed using a 1.5-T Siemens Sonata scanner (Erlangen, Germany) and a five-element cardiac array for signal reception. Short-axis balanced steady-state free precession (true FISP) short-axis cine images covering the entire LV (10 to 12 slices) were used to measure LV ESV (LVESV), LV end-diastolic volume (LVEDV), LV stroke volume (SV), and LV ejection fraction (EF). Image parameters were echo time =1.5 ms, repetition time = 3.0 ms, flip angle = 60°, slice thickness = 8 mm with a 2-mm gap between slices, matrix = 256 × 192, field of view = 300 to 380 mm, and 10 views per segment with 30 reconstructed cardiac phases. All image acquisitions were prospectively ECG gated and acquired during breath holds (10–15-s breath holds per slice).

cMRI tissue tagging was used to measure regional LV circumferential motion at four short-axis slice locations and to calculate circumferential strain, global twist and untwisting rates, regional twist and untwisting rates, and shear strains and strain rates (Fig. 1). The apical slice was prescribed 1 cm from the true apex, as identified from two-, three-, and four-chamber-long axis views, with each additional short-axis slice prescribed with a skip of 16 mm between the centers of slices. Typical image acquisition parameters were as follows: spoiled gradient-echo pulse sequence with echo time = 2.2 ms, repetition time = 4.0 ms, flip angle = 12°, slice thickness = 8 mm, matrix = 192 × 128, field of view = 300 to 380 mm, 600 Hz/pixel receiver bandwidth, and 5 views per segment for a 20-ms temporal resolution. The tissue tags were applied with a delay of 200 ms from the ECG trigger to ensure tag persistence throughout diastole (11). Blood pressure (automated cuff sphygmomanometer) and heart rate (ECG) were monitored throughout all acquisitions.

Data processing. Assessment of LV volumes was performed by manual segmentation of short-axis cine images at end diastole and end systole (Argus; Siemens Medical Systems). LVEDV and LVESV were calculated using Simpson's rule (26) and subsequently used to calculate SV and EF. Papillary muscles were included in the ventricular cavity, and LV mass was measured using the difference in endo- and epicardial volumes multiplied by a tissue density of 1.05 g/ml. The processing of tagged images to yield strains and rotations was performed with custom-automated software, developed using the Matlab programming environment, which has been detailed in previous publications (7, 20). Briefly, the images from all cardiac phases were morphed to a reference image to determine the spatial deformation field for the myocardium as a function of cardiac phase. User input was limited to tracing the endo- and epicardium at a single reference cardiac phase for each slice. The resulting spatial deformation field within the myocardium was used to calculate the targeted strain fields at all cardiac phases (18). The calculation of rotation and twist was similar to previously published methods (21) whereby the angle of rotation for each short-axis slice, ϕ, was calculated as the average rotation for all points in the slice about the LV centroid, which was calculated for each cardiac phase. Positive ϕ is counterclockwise when viewed from apex to base. The global LV twist, θ, was calculated as the difference between the counterclockwise (positive) rotation at the apex and clockwise rotation at the base (viewed from apex), $\theta = \phi_{apex} - \phi_{base}$. The rate of untwisting, $d\theta/dt$, was calculated as the discrete time derivative of the twist versus time curve. The peak twist parameters were calculated as the largest magnitudes of θ and $d\theta/dt$ during the appropriate time intervals. The time-varying rotation at apical and basal slices and the corresponding twist metrics averaged over all subjects are shown in Fig. 2. The time

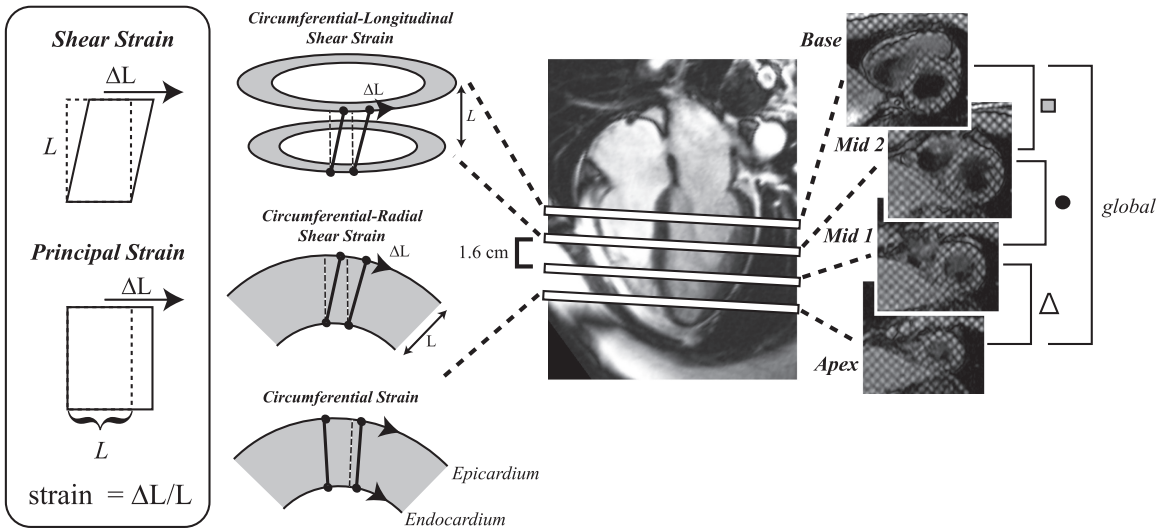

Fig. 1. Four evenly spaced short-axis grid-tagging slices between the base and apex are used to measure the global twist and rate of untwisting and the regional equivalents at basal (■), mid (●), and apical (△) locations. All strains were measured using the change in length, ΔL, per unit length, L, as shown in the *inset*. For circumferential strain, ΔL and L were measured in the circumferential direction. For circumferential-longitudinal shear strain (ϵ_{CL}), ΔL was the difference in circumferential displacement for slices separated by a longitudinal distance, L. For circumferential-radial shear strain (ϵ_{CR}), ΔL was the difference in circumferential displacement for epicardium and endocardium separated by a radial distance, L.

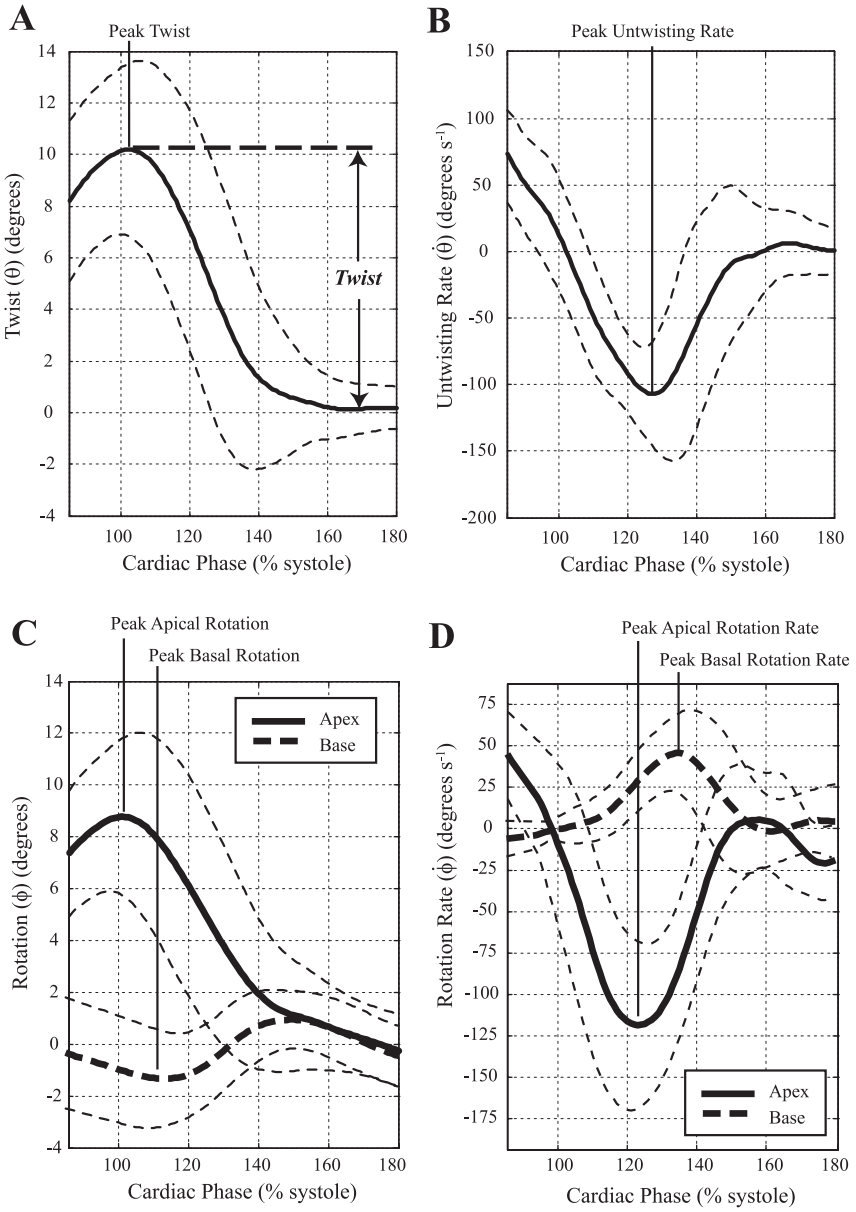

Fig. 2. Average twist (*A*), untwisting rate (*B*), and apical and basal rotation (*C*) and rotation rate curves (*D*) for the 32 subjects. The thin dashed lines show a range of ±1SD. As shown in *A*, twist is defined relative to the equilibrium values during diastasis before atrial contraction.

axes for all curves were normalized to the time of aortic valve closure and expressed as the percentage of systole, where 100% of systole is at the aortic valve closure.

The twist and untwisting measurements were repeated for each pair of adjacent short-axis slices at apical, midventricular, and basal levels of the LV, as shown in Fig. 1, which were defined as regional twist $\theta_{\text{apex, mid, or base}}$ and untwisting rates $d\theta/dt_{\text{apex, mid, or base}}$. All regional twist and untwisting rate values were normalized to the distance between slices and are thus in units of torsion (i.e., twist per cm). ϵ_{CL} and circumferential-radial shear strain (ϵ_{CR}) components were calculated using tissue displacements measured at the four short-axis slice locations (18). As shown in Fig. 1, ϵ_{CR} is related to the difference in endo- and epicardial rotation, whereas ϵ_{CL} is related to the difference in rotation in neighboring short-axis slices. ϵ_{CR} values were averaged over all circumferential locations within each short-axis slice location, yielding apex, mid-1, mid-2, and base values, as indicated in Fig. 1. ϵ_{CL} values were averaged for all radial and circumferential locations, for each pair of short-axis slices, yielding apex, mid, and base values, as indicated in Fig. 1. ϵ_{CL} calculations were also repeated for the use of only apical and basal slices, which are termed $\epsilon_{CL(Global)}$, and are thus similar to the calculation of conventional twist and untwisting rates but take the LV radius for each slice and distance between slices into consideration. Diastolic shear strain rates ($d\epsilon/dt$) were calculated as the time derivative of corresponding strains. Peak values (i.e., peak strain, peak twist, and peak untwisting rates) were reported for all calculated parameters. The relationship between all systolic shear strain and corresponding diastolic shear strain components was evaluated by normalization of diastolic rates to peak systolic strains and by linear correlation. All normalized values are identified using a subscript, for example, normalized untwisting rate is termed $d\theta/dt_{Norm} = d\theta/dt_{peak}/\theta_{peak}$ (in s^{-1}). Previously, the normalized untwisting rates have been defined as normalized rotation velocities (19) or untwisting performance (8, 19, 24).

Strain and twist values were measured with respect to a cardiac phase during diastasis, as shown in Fig. 2*A* (11), as opposed to the more conventional early systolic phase. This definition of strain reflects the fact that the effective or functional length of contracted myofibrils, related to their ability to store and release elastic energy and to drive the fiber lengthening and untwisting, is relative to the equilibrium fiber length (3, 30).

Statistics

Statistical analysis was performed using Microsoft Office Excel 2007 (Microsoft, Redmond, WA). Descriptive data are presented as means ± SD. Paired sample Student's *t*-tests were used for statistical comparisons between parameters. Least squares linear regression analysis was performed to correlate twist (or shear strain) and the corresponding untwisting rate (or shear strain rate) parameters. The *y*-intercept was set to zero for all linear regression analysis to allow for a direct comparison of the best-fit slope to the untwisting performance or strain rate performance metrics. Statistical significance was assigned for $P < 0.05$.

RESULTS

Global Function

Figure 2 shows the average apical and basal rotation (ϕ) and twist (θ) curves for the 32 subjects with corresponding SDs. The average of the peak values and timings for these two locations, as well as the mid-1 and mid-2 slice locations, is summarized in Table 2. The transition from positive to negative peak systolic rotation occurs between the mid-2 and basal slice locations. Mean peak twist was 10.4 ± 2.6° (6.8° to 17.1°) and the mean untwisting rates were −144.2 ± 34.9° s^{-1} (−90.0° s^{-1} to −220.6° s^{-1}) with a significant negative linear correlation between peak twist and untwisting rates ($R = -0.58$, $P < 0.001$), as shown in Fig. 3*A*. The average normalized untwisting rate ($d\theta/dt_{Norm}$) was −13.6 ± 2.1 s^{-1} (−10.0 to −19.7 s^{-1}). Corresponding systolic circumferential-longitudinal strain [$\epsilon_{CL(Global)}$], measured using the same apical and basal slice locations, was 0.06 ± 0.01 (0.037 to 0.082) with diastolic strain rates [$d\epsilon_{CL(Global)}/dt$] of 0.72 ± 0.13 s^{-1} (−0.45 to −1.0 s^{-1}), showing a significant negative linear correlation between systolic strain and diastolic strain rate ($R = -0.85$, $P < 0.001$) in Fig. 3*B*. The average normalized circumferential-longitudinal strain rate [$d\epsilon_{CL(Global)}/dt_{Norm}$] was −12.1 ± 1.4 s^{-1} (−10.1 to −14.3 s^{-1}). There was no significant correlation between untwisting rates and either LVESV or peak systolic circumferential strain as shown in Fig. 3, *C* and *D* ($P > 0.05$). Similarly, peak twist was not correlated with LVESV or peak circumferential strain, as shown in Fig. 3, *E* and *F* ($P > 0.05$). LVEDV, LV SV, and LV EF were also uncorrelated with peak twist and untwisting rates.

Table 2. *Apical and basal rotation and rotation rates and twist and untwisting rates*

Peak systolic rotation (base) (ϕ_{base}), degrees	−0.5 ± 1.4
Time of peak, ms	375 ± 38
%Systole	115 ± 8
Peak diastolic rotation rate (base) ($d\phi_{base}/dt$), degrees·s^{-1}	57.6 ± 22.8
Time of peak, ms	425 ± 41
%Systole	131 ± 9
Peak systolic rotation (mid-2) ($\phi_{mid\text{-}2}$), degrees	1.2 ± 2.4
Time of peak, ms	364 ± 43
%Systole	112 ± 9
Peak diastolic rotation rate (mid-2) ($d\phi_{mid\text{-}2}/dt$), degrees·s^{-1}	−3.2 ± 27.6
Time of peak, ms	400 ± 38
%Systole	123 ± 8
Peak systolic rotation (mid-1) ($\phi_{mid\text{-}1}$), degrees	6.1 ± 2.1
Time of peak, ms	325 ± 23
%Systole	100 ± 6
Peak diastolic rotation rate (mid-1) ($d\phi_{mid\text{-}1}/dt$), degrees·s^{-1}	−69.1 ± 26.3
Time of peak, ms	380 ± 31
%Systole	117 ± 8
Peak systolic rotation (apex) (ϕ_{apex}), degrees	9.7 ± 2.4
Time of peak, ms	328 ± 29*
%Systole	101 ± 8*
Peak diastolic rotation rate (apex) ($d\phi_{apex}/dt$), degrees·s^{-1}	−125.1 ± 42.2
Time of peak	394 ± 34*
%Systole	121 ± 11*
Peak systolic twist (θ), degrees	10.4 ± 2.6
Time of peak, ms	335 ± 29
%Systole	103 ± 7
Peak diastolic untwisting rate ($d\theta/dt$), degrees·s^{-1}	−144.2 ± 34.9
Time of peak, ms	412 ± 36
%Systole	126 ± 9

Values are means ± SD. *$P < 0.001$, difference from the times of peak basal rotation and rotation rate.

Regional Function

Figure 4 shows the average regional torsion (Fig. 4*A*), ϵ_{CL} (Fig. 4*B*), and ϵ_{CR} (Fig. 4*C*) curves for the 32 subjects. The SD for each of these parameters, calculated using all time points and locations, is shown on each graph. Figure 5 summarizes the mean peak systolic strains, diastolic strain rates, and normalized diastolic strain rates for torsion, circumferential-longitudinal, and circumferential-radial components for apical, mid, and basal locations. Figure 5, *A–C*, shows larger regional torsion and untwisting rates toward the apex ($P < 0.001$), but the normalized untwisting rates are similar at apical (−12.8 ± 2.6 s^{-1}), mid (−11.9 ± 1.3 s^{-1}), and basal (−13.5 ± 2.7 s^{-1}) locations. Figure 6*A* shows the individual peak regional torsion and untwisting rates for all 32 subjects and their significant linear relationship ($P < 0.05$), where the slope is equivalent to the normalized untwisting rate (i.e., the ratio of untwisting rates to the peak torsion). Table 3 summarizes the average normalized untwisting rates and normalized diastolic shear strain rates for all regional and global measurements in this study.

Figure 5, *D–F*, shows the corresponding average values for the systolic ϵ_{CL} component. In contrast to regional torsion and untwisting, the ϵ_{CL} systolic component has smaller values toward the apex ($P < 0.001$) with a similar pattern for the diastolic shear strain rate. The normalized diastolic strain rate [$d\epsilon_{CL}/dt_{Norm}$] was uniform from apex (−15.1 ± 6.5 s^{-1}) to mid (−14.9 ± 5.6 s^{-1}) to basal (−15.0 ± 3.9 s^{-1}) locations ($P > 0.05$; ANOVA). Figure 6*B* shows the individual regional circumferential-longitudinal strains and diastolic strain rates for all 32 subjects and their significant linear relationship ($P < 0.05$), where the slope is equivalent to $d\epsilon_{CL}/dt_{Norm}$ (regional average) in Table 3.

Finally, the variation in peak ϵ_{CR} and the corresponding diastolic strain rates from apex to base are shown in Fig. 5, *G–I*, with statistically significant differences between all locations ($P < 0.001$). The normalized diastolic strain rate, $d\epsilon_{CR}/dt_{Norm}$, was uniform from apex (−13.6 ± 5.9 s^{-1}) to mid-1 (−15.6 ± 7.7 s^{-1}) to mid-2 (−14.1 ± 10.2 s^{-1}) to basal (−14.5 ± 10.1 s^{-1}) locations ($P > 0.05$, ANOVA). Figure 6*C* shows the regional circumferential-radial strains and diastolic strain rates for all 32 subjects and their significant linear relationship ($P < 0.05$), with a reversal in sign from base to apex, where the slope of this relationship is equivalent to $d\epsilon_{CR}/dt_{Norm}$ (regional average) in Table 3.

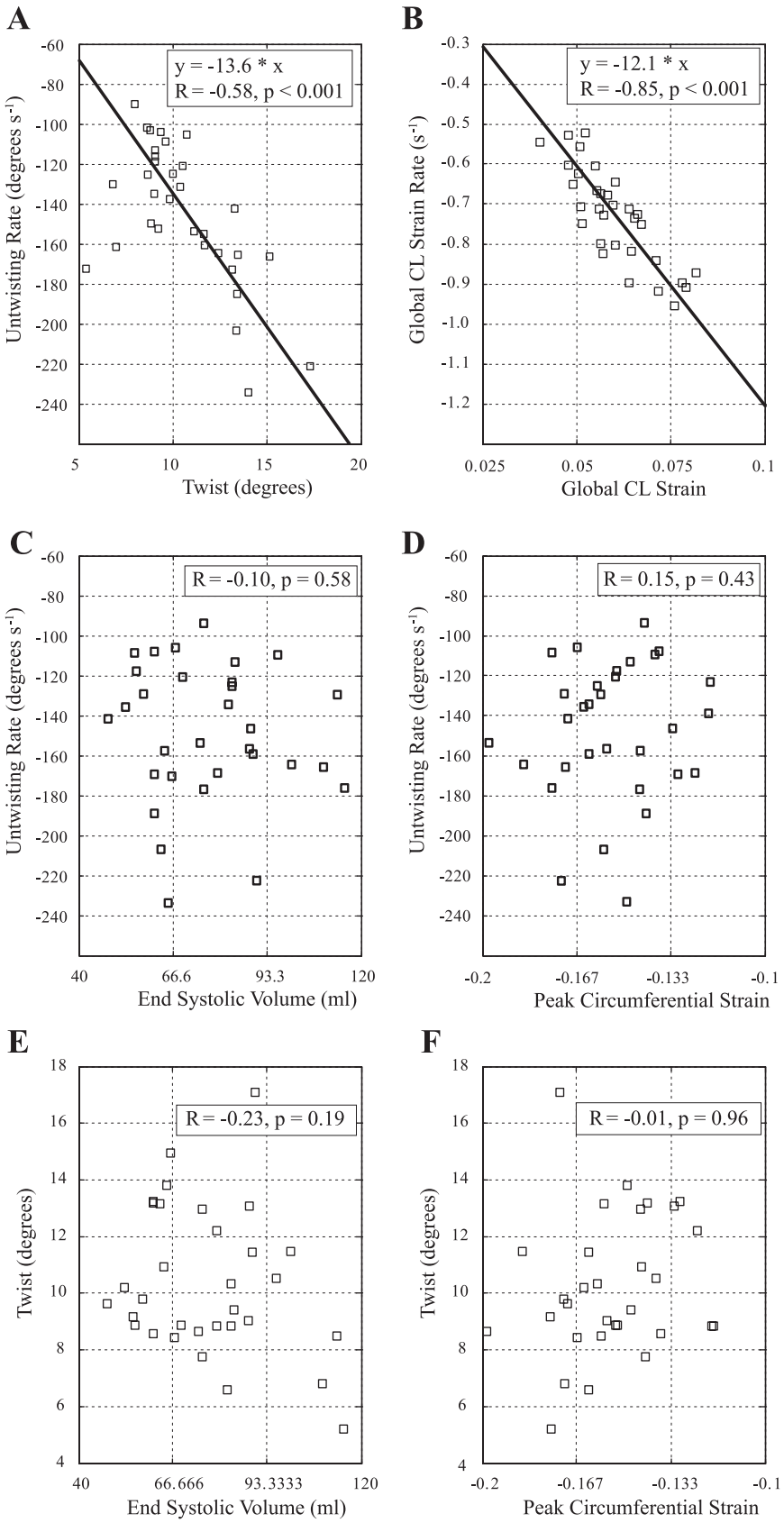

Fig. 3. In the 32 subjects, peak LV twist is significantly correlated with the peak untwisting rate (*A*), and the circumferential-longitudinal (CL) systolic shear strain (associated with systolic twist) is significantly correlated with the corresponding diastolic shear strain rate (associated with untwisting rate) (*B*). The peak rate of untwisting has no significant correlation with end-systolic volume (*C*) or peak circumferential strain (*D*) with similar results for peak twist in *E* and *F*.

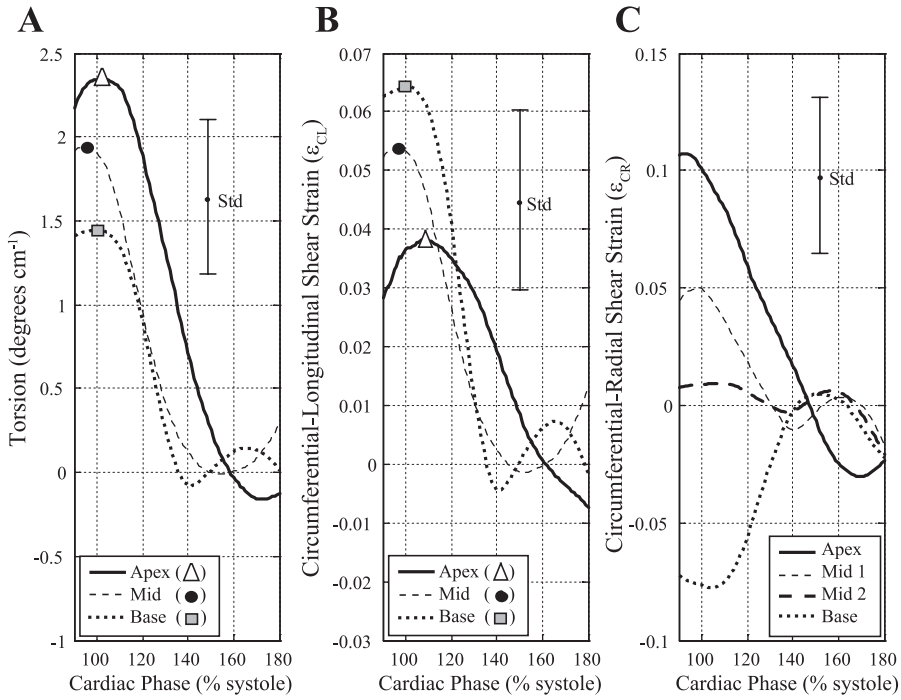

Fig. 4. Average torsion (*A*), ϵ_{CL} (*B*), and ϵ_{CR} (*C*) curves for the 32 subjects for apex, mid, and basal locations. The SD (Std) is shown for each parameter. The average of the peak values for each curve is summarized in Fig. 5.

DISCUSSION

LV untwisting is now a commonly evaluated parameter in studies of diastolic function. The purpose of this study was to characterize the relationship between the early diastolic strain rates, including the conventionally measured ventricular untwisting rates, with the preceding systolic shear strains in the healthy heart. The primary findings of this study are the linear correlations between the diastolic strain rates with the corresponding preceding systolic strains, for all strain components (torsion, ϵ_{CL}, and ϵ_{CR}) and for apical, mid, and basal ventricular regions. All measured strain components were shown to vary significantly from base to apex for both peak systolic strains and subsequent early diastolic strain rates with distinct spatial patterns for each of the torsion, ϵ_{CL}, and ϵ_{CR} components. Normalization of the diastolic rates to the peak systolic strains largely removed the spatial variations in shear strain rates and yielded similar values for all regions, as summarized in Table 3. These findings support a linear model of torsional recoil, where larger systolic strains are associated with proportionately larger early diastolic strain rates. The spatial uniformity of the normalized values suggests that recoil, as it is related to shear strains, is homogeneous over the healthy heart.

Our findings also show that peak twist and untwisting rates (and all early diastolic shear strain rates) are not significantly related to the extent of circumferential strain or ESV (Fig. 3, *C–F*). The potential independence of the principal and shear strain components as mechanisms for energy storage and for driving LV recoil (i.e., the release of energy stored in shortened elastic fibers) is plausible given the orthogonality of these components in the strain tensor. The uncoupling of shear strains and the principal strains has previously been observed as a dissociation of twist and volumetric LV function (9, 27) and is observed in all hearts during isovolumic relaxation when untwisting dominates changes in fiber length with ~40% of untwisting being completed (10, 12, 22) before changes in the principal strains or LV volume. Thus early diastolic (isovolumic) LV torsional recoil (or more generally, shear strain recoil) occurs with negligible changes in circumferential strain or volume and likely reflects the release of energy stored in systolic shear stain and not that stored in the principal strains, such as circumferential systolic strain. In contrast to our findings, the findings of Wang et al. (35) did show that untwisting rates are significantly correlated with both peak systolic twist and ESV in a population of patients with heart failure (35). Their findings may reflect a strong primary correlation between all systolic strain components in their population (i.e., a correlation between twist and ESV) and not a direct correlation between ESV and untwisting rates, although this was not directly evaluated in the study.

Regional Shear Strain

From Figs. 4*A* and 5, *A* and *B*, untwisting rates are larger toward the apex with spatially matched peak systolic torsion, yielding similar normalized untwisting rates from apex to base. Larger regional torsion at the apex has been previously reported (18). This spatial pattern was reversed for the circumferential-longitudinal shear strains. Thus, while the apex has the largest regional torsion over the length of the ventricle when the smaller apical radius is taken into consideration in the calculation of ϵ_{CL}, there is less shear strain at the apex, as shown in Figs. 4*B* and 5, *D* and *E*. Bogaert and Rademakers (4) reported a similar pattern with smaller ϵ_{CL} systolic strains measured at the apex. The corresponding diastolic ϵ_{CL} shear strain rates have not been previously reported. As shown in Fig. 5, *D* and *E*, the ϵ_{CL} systolic shear strains and diastolic strain rates are spatially matched, yielding similar normalized diastolic shear strain rates at all locations ($P > 0.05$). The circumferential-radial shear strains (related to the difference in endocardial and epicardial rotation) had significant variations from apex to base, again with spatial matching of the systolic

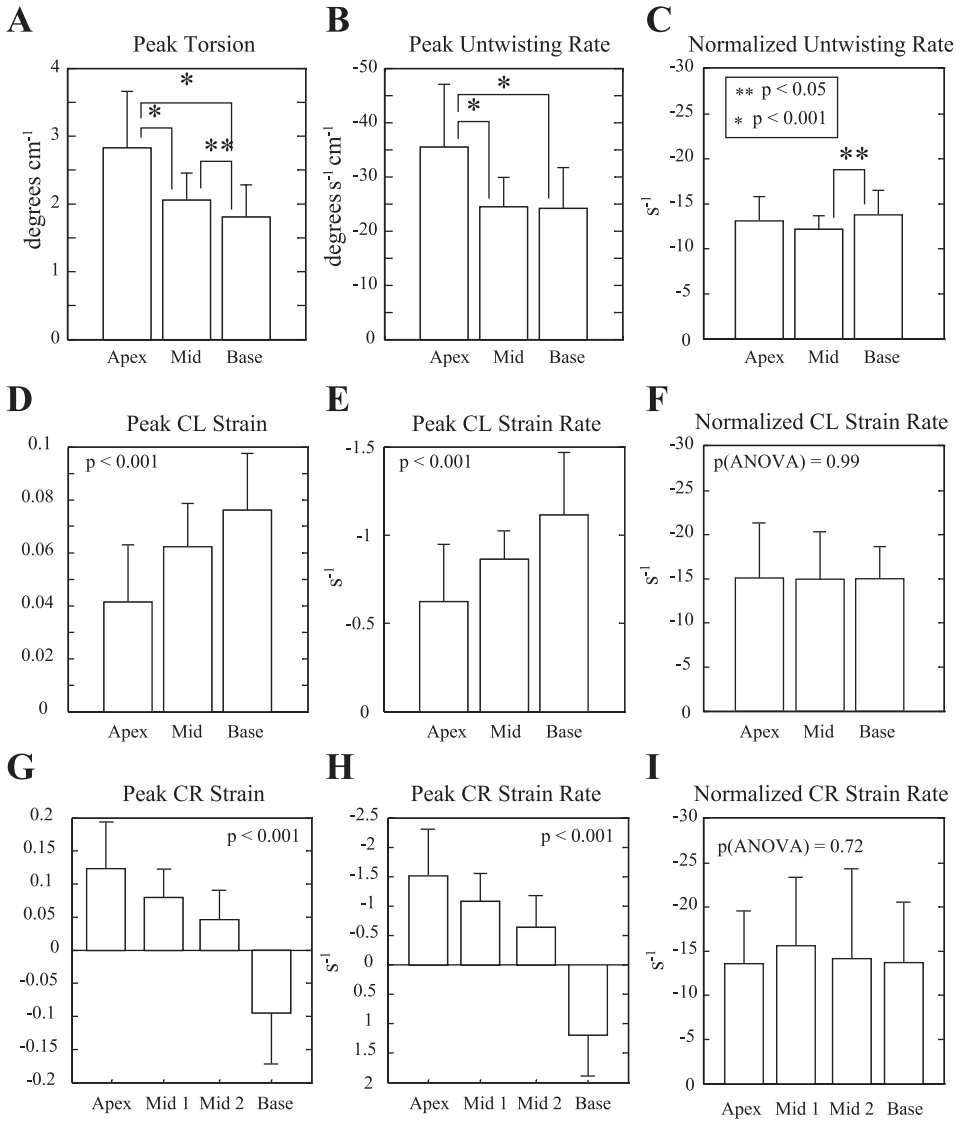

Fig. 5. *A*, *D*, and *G*: peak torsion, ϵ_{CL}, and ϵ_{CR} values in the 32 subjects, measured from apex to base. *B*, *E*, and *H*: the early diastolic peak rates of change for the strain components shown in *A*, *D*, and *G*, showing similar patterns as a function of position. *C*, *F*, and *I*: normalization of the diastolic rates (*B*, *E*, and *H*) to the peak systolic strain (*A*, *D*, and *G*) for each component yields a performance metric that is termed the untwisting performance or strain rate performance (with units in s^{-1}).

and diastolic values and thus similar normalized diastolic shear strain rates at all locations ($P > 0.05$). The pattern of ϵ_{CR} reversal from apex to base has been previously noted (4) with similar systolic shear strain values, but this is the first report of a similar pattern for the diastolic strain rates.

It is important to note in consideration of twist and shear strains that twist, unlike the strain metrics, does not provide a direct measure of changes in fiber length. Twist is most similar to the ϵ_{CL} component, both being related to the difference in rotation of parallel short-axis slices, but twist calculations do not take the magnitude of the ventricular radius or the change in radius over time into consideration as does ϵ_{CL}. These differences may account for the tighter correlation between the ϵ_{CL} and ϵ_{CL}/dt than was observed between twist and untwisting rates, as shown in Fig. 3, *B* and *A*, respectively. The ϵ_{CR} shear strain component measured in the current study is mathematically distinct from ϵ_{CL} and twist deformations, and thus the linear correlation between systolic ϵ_{CR} and early diastolic ϵ_{CR}/dt (Fig. 6*C*) provides an independent evaluation of the relationship between the systolic strains and diastolic strain rates and of torsion recoil.

Interpretation of Normalized Strain Rates

Linear relationships between systolic strain and diastolic strain rates (i.e., lengthening rates) have been observed in in vitro experiments on isolated rat cardiac myocytes (13). Furthermore, a modification of these isolated myocytes, with the application of trypsin to selectively degrade titin, was shown to reduce the slope of the peak strain rate versus the strain curve from 9 to 4.5 s^{-1} (i.e., equivalent to a reduction of the normalized strain rate). Reduced normalized strain rates with a degradation of titin most likely reflects the reduced capacity of the myocytes to store elastic energy. Specifically, it is trivial to show that the normalized diastolic strain rate for an idealized linear spring described by Hooke's Law, $F = -k(x - x_0)$, is equal to the natural frequency of the system, $\omega = k/m$, which is determined by the spring constant and mass of the system [F is the restoring force for a spring with a stiffness, k, with a mass, m, displaced from an equilibrium position (x_0) by a distance, x]. This result can be directly calculated from the position [i.e., strain, $x = x_0 \sin(\omega t)$] and velocity [i.e., strain rate, $dx/dt = x_0\omega \cos(\omega t)$] expressions, yielding a normalized

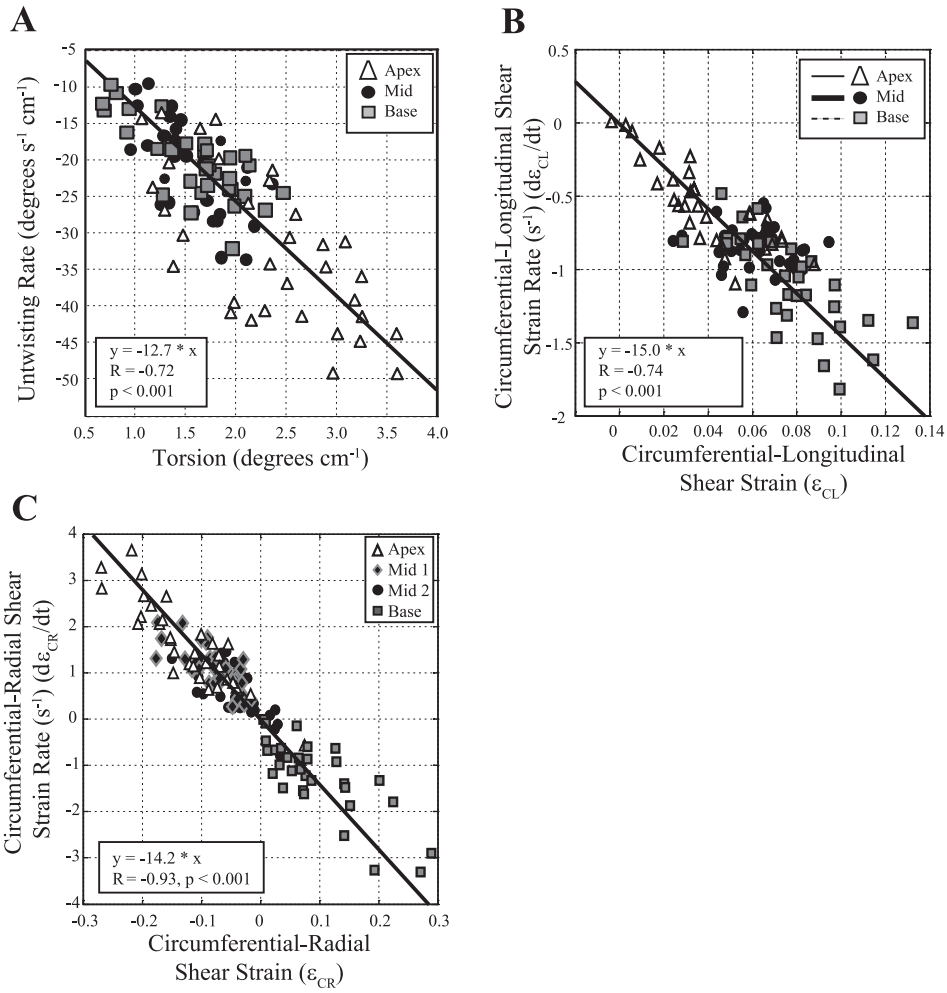

Fig. 6. Torsion and shear strain values are compared with strain rates in all 32 subjects. Mean values are summarized in Fig. 5. *A*: peak torsion (in twist/cm) at apical, mid, and basal locations are compared with the corresponding untwisting rates. *B*: the circumferential-longitudinal (ϵ_{CL}) shear strains and strain rates are significantly different at apex, mid, and base locations, and all regions show a similar negative correlation between strain and strain rates. *C*: the circumferential-radial (ϵ_{CR}) shear strains vary from negative values at the apex to positive values at the base with a significant negative correlation with the corresponding diastolic shear strain rates.

diastolic strain rate = $dx/dt_{peak}/x_{peak} = x_0\omega/x_0 = \omega$. The predominantly linear relationships between peak twist and untwisting rates (or shear strains and diastolic shear strain rates), illustrated in the current study, are consistent with the noted in vitro data and simplified mathematical models.

Previously, recoil models of ventricular function have shown that the rate of diastolic fiber lengthening is modulated by the viscoelastic material properties of the myocardium (2, 3, 13, 14), including the calcium-dependent actin-myosin disassociation (relaxation) (31). The normalized diastolic strain rates, including the normalized untwisting rates, are thus likely representative of the early diastolic viscoelastic properties of LV, where increased stiffness (referring here to the capacity of the myocardium to store elastic energy, elasticity) would yield higher normalized values. In contrast, the viscosity of the myocardium, which would include the effects of actomyosin inactivation (31), reflect the frictional forces that impede the release of this energy and would be expected to reduce the normalized strain rate values. For example, Nagel et al. (19) reported a reduction in "normalized rotation velocities," equivalent to the normalized untwisting rates in the current study, in patients with aortic valve stenosis. The authors proposed that smaller normalized rotation velocities were potentially reflective of the changes in collagen architecture, associated with increased viscosity and reduced elasticity, which is a well-known long-term consequence of aortic stenosis (33). More recently, Dalen et al. (8) showed a significant decrease in normalized peak diastolic untwisting velocity with advancing age, with an associated delay in the time of peak untwisting rate.

Limitations

All rotation and strain data in this study were evaluated from four short-axis slices. These images can be used to measure only the in-plane (circumferential and radial) motion, and thus the third shear strain component (longitudinal-radial) was not measured in this study. Also, the motion of the myocardium in the longitudinal (through-plane) direction will give rise to systematic errors in all measured tissue displacements for a static imaging plane, although it has been shown that two- and three-dimensional tagging yield highly correlated torsion values (28). To minimize errors from through-plane motion at the base and to avoid motion of the base out of the imaging plane during systole (i.e., the average longitudinal displacement of the base was 2.4 ± 0.4 cm in our population), the most basal slice was typically 2 to 3 cm from the true base, measured at end diastole. Also, because of variations in heart length in our study population (Table 2), the most basal slice location relative to the true base was not identical in all subjects, which

Table 3. *Normalized untwisting rates and shear strain rates (peak diastolic strain rates/peak systolic strains)*

Normalized untwisting rates ($d\theta/dt_{Norm}$)	
Global, s^{-1}	-13.6 ± 2.1*
Apex, s^{-1}	-12.8 ± 2.6‡
Mid, s^{-1}	-11.9 ± 1.3‡
Base, s^{-1}	-13.5 ± 2.7‡
Regional average, s^{-1}	-12.7 ± 2.4*
Normalized circumferential-longitudinal strain rates ($d\epsilon_{CL}/dt_{Norm}$)	
Global, s^{-1}	-12.1 ± 1.4†
Apex, s^{-1}	-15.0 ± 6.5§
Mid, s^{-1}	-14.9 ± 5.5§
Base, s^{-1}	-15.0 ± 3.9§
Regional average, s^{-1}	-15.0 ± 6.5†
Normalized circumferential-radial strain rates ($d\epsilon_{CR}/dt_{Norm}$)	
Apex, s^{-1}	-13.6 ± 5.9§
Mid-1, s^{-1}	-15.6 ± 7.7§
Mid-2, s^{-1}	-14.1 ± 10.2§
Base, s^{-1}	-13.7 ± 6.4§
Regional average, s^{-1}	-14.2 ± 7.7

Values are means ± SD. Slice locations used for the calculation of regional (apex, mid, and base) or global values are defined in Figure 1. *$P > 0.05$, global and regional average values are not significantly different; †$P < 0.001$, global values are less than average regional values; ‡$P < 0.05$, group means are different (ANOVA); §$P > 0.05$, group means are not different (ANOVA).

is thus a source of systematic error in our study as some overlap between regions. Despite this overlap, all regional twist and shear strains and diastolic strain rates were significantly different between all regions.

The spatial variations in twist and shear strains were measured only as a function of position from apex to base, although it is well known that peak shear strains also vary from endo- to epicardium and with circumferential location (4, 18). Also, all rotation, twist, and strain measurements were calculated with respect to diastasis and not with respect to the more commonly used end-diastolic reference, which are separated by the effects of the late atrial contraction. This alternate reference will not affect the rate of change measurements (untwisting rates, strain rates), but it may result in slightly lower peak twist and strain values, because the diastasis-reference approach does not include the effects of the atrial contraction. The slightly lower peak systolic strains would be expected to give rise to larger normalized parameters. Accordingly, our normalized untwisting rates of -13.6 ± 2.1 s^{-1} are larger than the previously reported values, which are approximately -11 s^{-1} (8, 19, 24). A diastasis reference was used in this study to better reflect the mechanisms of recoil, which are based on the release of stored energy relative to the resting configuration of the fibers and to ensure MRI tag persistence throughout diastole. While it is not possible to directly measure the resting fiber length, nor is it agreed upon at which point in the cardiac cycle (or which volume) equilibrium occurs (37), diastasis is a better representation of this equilibrium than is end diastole. Finally, the findings of the current study are limited to the healthy heart in younger men.

Conclusion

In summary, the early diastolic shear strain rates ($d\epsilon_{CL}/dt$ and $d\epsilon_{CR}/dt$) and untwisting rates ($d\theta/dt$) were shown to vary significantly from apex to base, and all components were linearly correlated with their corresponding systolic strains. Direct normalization of the diastolic shear strain rates by the peak systolic strains (or untwisting rates to peak twist) yielded a uniform measure of diastolic function that was similar between the distinct shear strain and twist components and similar at apical, mid, and basal ventricular positions. These results suggest that torsional recoil can be described with a linear model in the healthy heart, where systolic shear strain gives rise to a proportional early diastolic shear strain rates, independent of measurement location. They further suggest that spatial heterogeneity in diastolic shear strain rates are likely the consequence of nonuniform systolic function. The diastolic shear strain rates and untwisting rates were not significantly correlated with the systolic circumferential strains or ESV or EDV, which suggests that torsional recoil, or more generally shear strain recoil, is uncoupled from the changes in fiber length associated with changes in volume.

ACKNOWLEDGMENTS

R. B. Thompson is an Alberta Heritage Foundation for Medical Research Scholar.

GRANTS

M. J. Haykowsky has a career award from the Canadian Institutes of Health Research. K. Chow, J. Cheng-Baron, J. M. Scott, and B. T. Esch were supported by doctoral graduate scholarships from the Natural Sciences and Engineering Research Council of Canada.

DISCLOSURES

No conflicts of interest, financial or otherwise, are declared by the author(s).

REFERENCES

1. **Arts T, Veenstra PC, Reneman RS.** Epicardial deformation and left ventricular wall mechanisms during ejection in the dog. *Am J Physiol Heart Circ Physiol* 243: H379–H390, 1982.
2. **Ashikaga H, Criscione JC, Omens JH, Covell JW, Ingels NB Jr.** Transmural left ventricular mechanics underlying torsional recoil during relaxation. *Am J Physiol Heart Circ Physiol* 286: H640–H647, 2004.
3. **Bell SP, Nyland L, Tischler MD, McNabb M, Granzier H, LeWinter MM.** Alterations in the determinants of diastolic suction during pacing tachycardia. *Circ Res* 87: 235–240, 2000.
4. **Bogaert J, Rademakers FE.** Regional nonuniformity of normal adult human left ventricle. *Am J Physiol Heart Circ Physiol* 280: H610–H620, 2001.
5. **Burns AT, La Gerche A, Prior DL, Macisaac AI.** Left ventricular untwisting is an important determinant of early diastolic function. *JACC Cardiovasc Imaging* 2: 709–716, 2009.
6. **Chemla D, Coirault C, Hebert JL, Lecarpentier Y.** Mechanics of relaxation of the human heart. *News Physiol Sci* 15: 78–83, 2000.
7. **Cheng-Baron J, Chow K, Khoo NS, Esch BT, Scott JM, Haykowsky MJ, Tyberg JV, Thompson RB.** Measurements of changes in left ventricular volume, strain, and twist during isovolumic relaxation using MRI. *Am J Physiol Heart Circ Physiol* 298: H1908–H1918, 2010.
8. **Dalen BM, Soliman OI, Kauer F, Vletter WB, Zwaan HB, Cate FJ, Geleijnse ML.** Alterations in left ventricular untwisting with ageing. *Circ J* 74: 101–108, 2010.
9. **Dong SJ, Hees PS, Huang WM, Buffer SA Jr, Weiss JL, Shapiro EP.** Independent effects of preload, afterload, and contractility on left ventricular torsion. *Am J Physiol Heart Circ Physiol* 277: H1053–H1060, 1999.
10. **Dong SJ, Hees PS, Siu CO, Weiss JL, Shapiro EP.** MRI assessment of LV relaxation by untwisting rate: a new isovolumic phase measure of τ. *Am J Physiol Heart Circ Physiol* 281: H2002–H2009, 2001.
11. **Dorfman TA, Rosen BD, Perhonen MA, Tillery T, McColl R, Peshock RM, Levine BD.** Diastolic suction is impaired by bed rest: MRI tagging studies of diastolic untwisting. *J Appl Physiol* 104: 1037–1044, 2008.
12. **Esch BT, Scott JM, Warburton DE, Thompson R, Taylor D, Baron JC, Paterson I, Haykowsky MJ.** Left ventricular torsion and untwisting

during exercise in heart transplant recipients. *J Physiol* 587: 2375–2386, 2009.
13. **Helmes M, Lim CC, Liao R, Bharti A, Cui L, Sawyer DB.** Titin determines the Frank-Starling relation in early diastole. *J Gen Physiol* 121: 97–110, 2003.
14. **Helmes M, Trombitas K, Granzier H.** Titin develops restoring force in rat cardiac myocytes. *Circ Res* 79: 619–626, 1996.
15. **Ingels NB Jr, Hansen DE, Daughters GT 2nd, Stinson EB, Alderman EL, Miller DC.** Relation between longitudinal, circumferential, and oblique shortening and torsional deformation in the left ventricle of the transplanted human heart. *Circ Res* 64: 915–927, 1989.
16. **Jin SM, Noh CI, Bae EJ, Choi JY, Yun YS.** Decreased left ventricular torsion and untwisting in children with dilated cardiomyopathy. *J Korean Med Sci* 22: 633–640, 2007.
17. **Moon MR, Ingels NB Jr, Daughters GT 2nd, Stinson EB, Hansen DE, Miller DC.** Alterations in left ventricular twist mechanics with inotropic stimulation and volume loading in human subjects. *Circulation* 89: 142–150, 1994.
18. **Moore CC, Lugo-Olivieri CH, McVeigh ER, Zerhouni EA.** Three-dimensional systolic strain patterns in the normal human left ventricle: characterization with tagged MR imaging. *Radiology* 214: 453–466, 2000.
19. **Nagel E, Stuber M, Burkhard B, Fischer SE, Scheidegger MB, Boesiger P, Hess OM.** Cardiac rotation and relaxation in patients with aortic valve stenosis. *Eur Heart J* 21: 582–589, 2000.
20. **Nelson MD, Haykowsky MJ, Petersen SR, Delorey DS, Cheng-Baron J, Thompson RB.** Increased left ventricular twist, untwisting rates, and suction maintain global diastolic function during passive heat stress in humans. *Am J Physiol Heart Circ Physiol* 298: H930–H937, 2010.
21. **Notomi Y, Lysyansky P, Setser RM, Shiota T, Popovic ZB, Martin-Miklovic MG, Weaver JA, Oryszak SJ, Greenberg NL, White RD, Thomas JD.** Measurement of ventricular torsion by two-dimensional ultrasound speckle tracking imaging. *J Am Coll Cardiol* 45: 2034–2041, 2005.
22. **Notomi Y, Martin-Miklovic MG, Oryszak SJ, Shiota T, Deserranno D, Popovic ZB, Garcia MJ, Greenberg NL, Thomas JD.** Enhanced ventricular untwisting during exercise: a mechanistic manifestation of elastic recoil described by Doppler tissue imaging. *Circulation* 113: 2524–2533, 2006.
23. **Notomi Y, Popovic ZB, Yamada H, Wallick DW, Martin MG, Oryszak SJ, Shiota T, Greenberg NL, Thomas JD.** Ventricular untwisting: a temporal link between left ventricular relaxation and suction. *Am J Physiol Heart Circ Physiol* 294: H505–H513, 2008.
24. **Notomi Y, Srinath G, Shiota T, Martin-Miklovic MG, Beachler L, Howell K, Oryszak SJ, Deserranno DG, Freed AD, Greenberg NL, Younoszai A, Thomas JD.** Maturational and adaptive modulation of left ventricular torsional biomechanics: Doppler tissue imaging observation from infancy to adulthood. *Circulation* 113: 2534–2541, 2006.
25. **Nottin S, Doucende G, Schuster-Beck I, Dauzat M, Obert P.** Alteration in left ventricular normal and shear strains evaluated by 2D-strain echocardiography in the athlete's heart. *J Physiol* 586: 4721–4733, 2008.
26. **Peshock RM, Willett DL, Sayad DE, Hundley WG, Chwialkowski MC, Clarke GD, Parkey RW.** Quantitative MR imaging of the heart. *Magn Reson Imaging Clin N Am* 4: 287–305, 1996.
27. **Rademakers FE, Buchalter MB, Rogers WJ, Zerhouni EA, Weisfeldt ML, Weiss JL, Shapiro EP.** Dissociation between left ventricular untwisting and filling. Accentuation by catecholamines. *Circulation* 85: 1572–1581, 1992.
28. **Russel IK, Tecelao SR, Kuijer JP, Heethaar RM, Marcus JT.** Comparison of 2D and 3D calculation of left ventricular torsion as circumferential-longitudinal shear angle using cardiovascular magnetic resonance tagging. *J Cardiovasc Magn Reson* 11: 8, 2009.
29. **Sengupta PP, Khandheria BK, Narula J.** Twist and untwist mechanics of the left ventricle. *Heart Fail Clin* 4: 315–324, 2008.
30. **Sonnenblick EH.** The structural basis and importance of restoring forces and elastic recoil for the filling of the heart. *Eur Heart J* Suppl A: 107–110, 1980.
31. **Stuyvers BD, Miura M, ter Keurs HE.** Dynamics of viscoelastic properties of rat cardiac sarcomeres during the diastolic interval: involvement of Ca^{2+}. *J Physiol* 502: 661–677, 1997.
32. **Tan YT, Wenzelburger F, Lee E, Heatlie G, Leyva F, Patel K, Frenneaux M, Sanderson JE.** The pathophysiology of heart failure with normal ejection fraction: exercise echocardiography reveals complex abnormalities of both systolic and diastolic ventricular function involving torsion, untwist, and longitudinal motion. *J Am Coll Cardiol* 54: 36–46, 2009.
33. **Villari B, Campbell SE, Hess OM, Mall G, Vassalli G, Weber KT, Krayenbuehl HP.** Influence of collagen network on left ventricular systolic and diastolic function in aortic valve disease. *J Am Coll Cardiol* 22: 1477–1484, 1993.
34. **Wang J, Khoury DS, Kurrelmeyer K, Torre-Amione G, Nagueh SF.** Assessment of left ventricular relaxation by untwisting rate based on different algorithms. *J Am Soc Echocardiogr* 22: 1040–1046, 2009.
35. **Wang J, Khoury DS, Yue Y, Torre-Amione G, Nagueh SF.** Left ventricular untwisting rate by speckle tracking echocardiography. *Circulation* 116: 2580–2586, 2007.
36. **Yun KL, Niczyporuk MA, Daughters GT 2nd, Ingels NB Jr, Stinson EB, Alderman EL, Hansen DE, Miller DC.** Alterations in left ventricular diastolic twist mechanics during acute human cardiac allograft rejection. *Circulation* 83: 962–973, 1991.
37. **Zhang W, Chung CS, Shmuylovich L, Kovacs SJ.** Is left ventricular volume during diastasis the real equilibrium volume, and what is its relationship to diastolic suction? *J Appl Physiol* 105: 1012–1014, 2008.